Salinity-dependent diatom biosilicification implies an important role of external ionic strength

Engel G. Vrieling*†, Qianyao Sun‡, Mingwen Tian§, Patricia J. Kooyman¶, Winfried W. C. Gieskes‖, Rutger A. van Santen, and Nico A. J. M. Sommerdijk††**

*Groningen Biomolecular Sciences and Biotechnology Institute and ‖Department of Ocean Ecosystems, Center for Ecological and Evolutionary Studies, University of Groningen, P.O. Box 14, NL-9750 AA Haren, The Netherlands; ‡State Key Laboratory of Heavy Oil Processing, China University of Petroleum, Beijing 102249, China; §Nano Technology Instruments, Europe BV, Arnhemseweg 34, NL-7331 BL Apeldoorn, The Netherlands; ¶DelftChemTech and National Centre for High Resolution Electron Microscopy, Delft University of Technology, Julianalaan 136, NL-2628 BL Delft, The Netherlands; and **Schuit Institute of Catalysis and ††Soft Matter Cryo-Transmission Electron Microscopy Unit, Department of Biomedical Engineering, Eindhoven Technical University, P.O. Box 513, NL-5600 MB Eindhoven, The Netherlands

Edited by Richard Gordon, University of Manitoba, Winnipeg, MB, Canada, and accepted by the Editorial Board May 9, 2007 (received for review October 12, 2006)

The role of external ionic strength in diatom biosilica formation was assessed by monitoring the nanostructural changes in the biosilica of the two marine diatom species *Thalassiosira punctigera* and *Thalassiosira weissflogii* that was obtained from cultures grown at two distinct salinities. Using physicochemical methods, we found that at lower salinity the specific surface area, the fractal dimensions, and the size of mesopores present in the biosilica decreased. Diatom biosilica appears to be denser at the lower salinity that was applied. This phenomenon can be explained by assuming aggregation of smaller coalescing silica particles inside the silica deposition vesicle, which would be in line with principles in silica chemistry. Apparently, external ionic strength has an important effect on diatom biosilica formation, making it tempting to propose that uptake of silicic acid and other external ions may take place simultaneously. Uptake and transport of reactants in the proximity of the expanding silica deposition vesicle, by (macro)pinocytosis, are more likely than intracellular stabilization and transport of silica precursors at the high concentrations that are necessary for the formation of the siliceous frustule components.

biosilica | silica nanostructure | silicification | silica chemistry

Diatoms are known for the intriguing species-specific morphology of their siliceous exoskeletons, the frustules (1, 2), which consist of two silica valves (the epi- and hypovalve), siliceous girdle bands, and a protective organic casing that prevents dissolution of the siliceous parts in the aquatic environment. During cell division, a parental diatom cell undergoes cytokinesis, and each of the next two daughter cells produces a new hypovalve, a hypocingulum, and girdle band(s); the sequence of their formation differs among species (1, 2). After valve and girdle band completion, the daughter cells finally separate, and cell division continues. The silica of every new valve is formed in the silica deposition vesicle (SDV) that is located inside each daughter cell and is closely appressed to the plasma membrane along the cleavage furrow. The SDV rapidly expands two-dimensionally and subsequently thickens more slowly in the three-dimensional direction during formation of the new hypovalve (3, 4). In the course of this fast two-dimensional expansion process, the essential reactants for silica polymerization have to be transported efficiently to the SDV. Silicon transporters have been identified (5, 6), but there is no clear evidence that they transport sufficient amounts of silicic acid across the plasma membrane and/or SDV membrane to enable silica polymerization.

In diatoms, both organic and inorganic compounds foster silica biomineralization and possibly control silica precipitation and direct the structures formed (7–9). Relevant organic compounds are silica-precipitating peptides such as silaffins and long-chain polyamines (8–10). They all have an intracellular origin and require specific targeting or intracellular transport (11). Of the inorganic SDV constituents, silica precursors are most important. Diatom cells appear to contain high levels of reactive silica (12), but a cytosolic or compartmentalized intracellular location that harbors such concentrations has never been found. So, the question remains whether the reactive and soluble silica is stored in the cytosol after uptake or whether it is imported directly in or transported to the expanding SDV during valve formation. In the latter case, ions, cotransported by symport (13), also could enter the SDV and therewith directly change the reaction conditions for silica polymerization. The presence of a membrane potential or proton gradient over the SDV membrane has also been demonstrated by molecular probing (14). The importance of ionic strength in silica polymerization has been demonstrated already. Phosphate not only enhances *in vitro* silica precipitation mediated by polyamines but also controls the size of the silica particles formed (9, 10). It has also been demonstrated that the silica content of diatom cells differs significantly between marine and freshwater species (15); even within a single species the silica content depends on the salinity of the natural habitat or culture medium (16, 17). Whether or not this finding has implications for the biosilica nanostructure is not known. The occurrence of salinity-dependent nanostructural changes in diatom biosilica is of importance to a further understanding of the concerted action of biological and physicochemical processes involved in silicon biomineralization in diatoms; for oceanographers and biogeochemists, the effect of salinity on nanostructure and cellular silica content is valuable to assess species abundance and vertical distribution as well as cycling of elements in natural habitats. To investigate the relation between ionic strength of the environment and the diatom biosilica nanostructure, centric marine species *Thalassiosira punctigera* and *Thalassiosira weissflogii* were cultured at two distinct salinities, and their biosilica was subsequently subjected to detailed analysis of physicochemical properties by biophysical methods.

Results and Discussion

After preadaptation of two generations, growth rates of both *T. punctigera* and *T. weissflogii* were determined; next, each species

Author contributions: E.G.V. and Q.S. contributed equally to this work; E.G.V. designed research; E.G.V., Q.S., M.T., and P.J.K. performed research; E.G.V., Q.S., M.T., P.J.K., W.W.C.G., R.A.v.S., and N.A.J.M.S. analyzed data; and E.G.V., Q.S., M.T., P.J.K., W.W.C.G., R.A.v.S., and N.A.J.M.S. wrote the paper.

The authors declare no conflict of interest.

This article is a PNAS Direct Submission. R.G. is a guest editor invited by the Editorial Board.

Abbreviations: AFM, atomic force microscopy; BET, Brunauer–Emmett–Teller; BJH, Barrett–Joyner–Halenda; HR TEM, high-resolution transmission electron microscopy; psu, practical salinity units; SAXS, small angle x-ray scattering; SDV, silica deposition vesicle; USAXS, ultrasmall angle x-ray scattering.

†To whom correspondence should be addressed. E-mail: e.g.vrieling@rug.nl.

Table 1. Overview of structural and physicochemical properties of silicas obtained from the diatoms *T. punctigera* and *T. weissflogii* cultured at two distinct salinities and chemically prepared silicas at comparable salinities

Species	Salinity, psu*	Growth rate, div·day^{-1}	BET-specific surface area, m^2·g^{-1}	BJH pore dimension, nm	Pore dimension(s), nm†			Fractal dimension, D_s‡	
					EM	SAXS	USAXS	SAXS	USAXS
T. punctigera	20	0.264	12	10	—	10.3	62.8	3.3	2.5
				27–35	25–35	33.0	287		
	33	0.273	27	3	2.9	13.5	72.1	3.6	2.5
				30–45	30–40	38.5	379		
T. weissflogii	20	0.247	32	3.6	—	8.5	476	2.9	2.3
				35–45	25–35	28			
	33	0.238	39	3.7	3.6	10	600	3.2	2.5
				32–40	35–40	35			
Synthetic silica	0	NA	462.3	3.6	ND	ND	ND	ND	ND
	20	NA	298.5	3.6	ND	8.0	ND	2.6	ND
				5.3					
Synthetic silica	33	NA	266.8	3.8	ND	8.5	ND	3.0	ND
				33					

—, not detected; NA, not applicable; ND, not determined.
*psu, practical salinity units.
†Pore dimensions were calculated from transition points between straight scattering regions in the SAXS and USAXS spectra (22, 23).
‡Fractal dimensions were determined from the slopes of the straight scattering regions in the SAXS and USAXS spectra (22, 23).

was compared with respect to the two applied salinities (Table 1) to exclude the occurrence of impaired growth. Indeed, reduction in growth rate increases the cellular biogenic silica content (18). ANOVA analysis of growth for both species indicated that there was no significant difference in growth between the two applied salinities; apparently, growth was not hampered, so changes in biogenic silica content as a consequence of a reduced growth rate could be excluded. Including the preadaptation, at least six generations developed, and >98% of the harvested biosilica resulted from silicification during growth under both salinity regimes. Therewith, an accurate analysis of the physicochemical properties of the obtained biosilicas was assured.

The diatom biosilica harvested from the cultures was acid-cleaned for removal of external organic matter. High-resolution transmission electron microscopy (HR TEM) and atomic force microscopy (AFM) clearly demonstrated nanostructural (<100 nm) properties that varied with salinity (Fig. 1 and Table 1). Macromorphological changes were also observed. These changes were clearest in the biosilica of *T. punctigera*, of which the "walls" of the characteristic honeycomb structures were much more pronounced at lower salinity (Fig. 1*e*) than at higher salinity (Fig. 1*a*). In both *T. punctigera* and *T. weissflogii*, the silica appeared to be denser at the lower salinity [practical salinity units (psu) 20], and smaller discernable silica particles were present at the surface of the silica; for *T. weissflogii* the surface roughness clearly increased at lower salinity (Fig. 1 *d* and *h*). It is known from classical silica chemistry (19, 20) that smaller silica particles aggregate more tightly at a lower salinity while voids between the coalesced particles disappear. As a matter of fact, the size of the species-specific pores (for comparison, see Fig. 1 *b* and *f*) inside the silica became smaller or even disappeared in

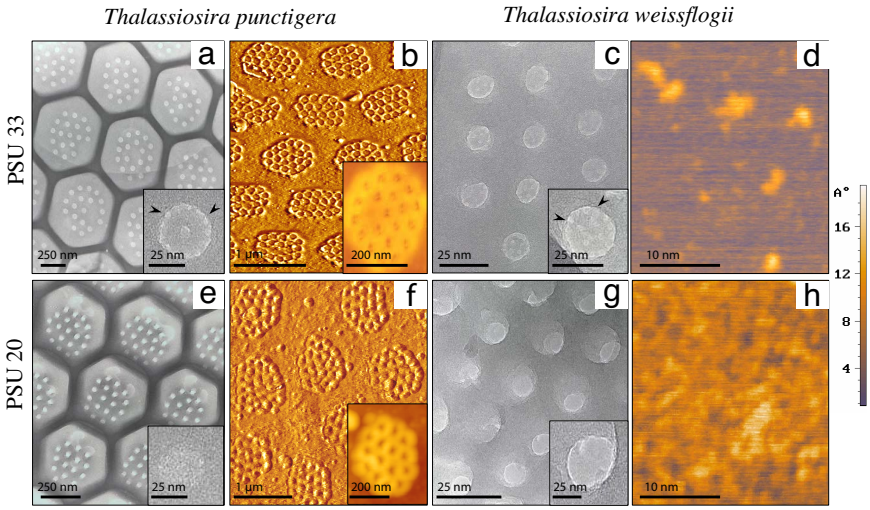

Fig. 1. Overview of nanostructural observations made by HR TEM and AFM of biosilica obtained from the diatoms *T. punctigera* (*a*, *b*, e, and *f*) and *T. weissflogii* (*c*, *d*, *g*, and *h*). (*Upper*) Samples from cells cultured at high salinity (psu 33). (*Lower*) Samples from cells cultured at low salinity (psu 20). (*Insets*) Higher magnifications of sieve-like silica structures with pores of 2.9 and 3.6 nm in diameter for, respectively, *T. punctigera* and *T. weissflogii* (arrowheads in *a* and *c* *Insets*) for biosilica formed at psu 33; these pores were absent at psu 20 (*e* and *g* *Insets*). (Scale bars, as indicated.) The intensity bar at the right reflects the specimen height (in Å).

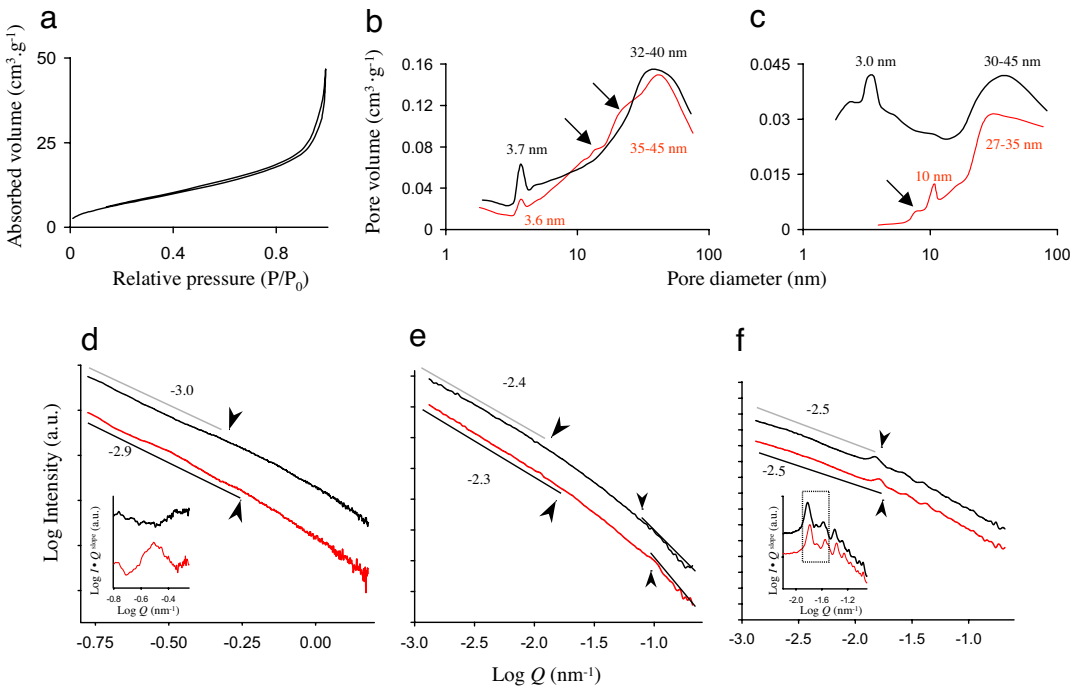

Fig. 2. Overview of data obtained from N_2-sorption/desorption analysis (*Upper*) and USAXS studies (*Lower*) on biosilica obtained from the diatoms *T. punctigera* and *T. weissflogii*. The black and red lines represent data of high and low salinity, respectively. (*a*) Sorption/desorption isotherm for *T. weissflogii*, with a narrow hysteresis loop, which is typical for mesoporous diatom biosilica (23). (*b* and *c*) BJH plots of the relative pore volume contributions of dominant well defined pores of *T. weissflogii* and *T. punctigera*. (*d* and *e*) SAXS and USAXS spectra of *T. weissflogii*. (*f*) USAXS spectrum of *T. punctigera*, showing distinct straight regions (some of which are indicated by a gray line) and typical transition points (arrowheads) between such regions. (*d* and *e Insets*) Oscillation patterns, after correction of descending (U)SAXS spectra.

case of the smallest pores. For *T. punctigera*, the diameter of the larger species-specific pores, which are present in well defined clusters, was estimated to be 69 nm (±1 nm) for silica of cells grown at psu 33 (Fig. 1*b*) and 59 nm (± 1.5 nm) for silica of cells grown at psu 20 (Fig. 1*f*). At certain locations, the smallest pores (Fig. 1 *a* and *c Insets*, arrowheads) had even disappeared. In *T. punctigera* (Fig. 1 *a* and *e Insets*) the pores of about 2.9 nm present at PSU 33 were not seen at PSU 20. This phenomenon was also observed for *T. weissflogii* where the pores of 3.6 nm disappeared at lower salinity (Fig. 1 *c* and *g Insets*).

Brunauer–Emmett–Teller (BET) N_2-sorption/desorption analyses of the specific surface area and subsequent calculations of the pore volume contributions using the Barret–Joyner–Harret (BJH) method (21) confirmed the microscopic observations (Fig. 2 *a–c* and Table 1). All obtained sorption/desorption curves revealed narrow hysteresis loops (Fig. 2*a*) that are characteristic for mesoporous silica with a low specific surface area (21). The specific surface area, however, clearly differed with the salinity conditions in both species (Table 1); the lower areas, found for silica obtained from cells cultured at lower salinity, could be ascribed to a decrease in voids between more tightly packed silica caused by lack of hydration (19, 20). BJH analysis of the pore volume (Fig. 2 *b* and *c*) revealed distinct peaks ascribed to the pores that contribute most to the total pore volume and confirmed that pores became smaller at lower salinity. The observation that in *T. punctigera* biosilica the pores of about 3 nm at psu 33 disappeared completely at psu 20 (Fig. 2*c*) was in line with the HR TEM observations and agreed with densification of the silica at lower salinity. In *T. punctigera*, the larger pores in the range of 30–45 nm at psu 33 had separated into two distinct size clusters of, respectively, 10 and 27–35 nm at psu 20 (Fig. 2*c*). The 10-nm pores most probably originated from denser packed silica particles that are smaller in contrast to the ones that collide at psu 33 and then form larger pores (the broader peak at 30–45 nm; Fig. 2*c*). The ≈10-nm shift toward smaller pores coincided with the observations made by AFM (Fig. 1). In *T. weissflogii*, the shift toward smaller pores was evident, albeit less clear-cut (Fig. 2*b*). At psu 20 the smallest pores (≈3.7 nm in size) did not disappear completely, but they evidently contributed less to the total pore volume with pores, being just slightly smaller at 3.6 nm. The shoulders (arrows in Fig. 2*b*) in the BJH plots also confirmed that pores of the biosilica of *T. weissflogii* became smaller at the expense of larger pores (32–40 nm) present in the broad peak at psu 33; again, shifts of ≈10 nm were observed.

Small- and ultrasmall-angle x-ray scattering studies (SAXS and USAXS, respectively) on the fractal and structural properties in the range of 3–60 nm (SAXS) and 60–6,200 nm (USAXS) confirmed the relation between external salinity and diatom biosilica nanostructure (Fig. 2 *d–f* and Table 1). (U)SAXS analysis indicated that within a single species the scattering spectra were different for the silicas obtained at psu 33 and psu 20, respectively (Fig. 2 *d–f*). In *T. weissflogii* (Fig. 2 *d* and *e*) the slopes of the typically straight scattering regions (22, 23) were less steep for the silica obtained at psu 20, corresponding to an increase in fractality denoted by the surface fractal dimension D_s [Table 1; with $D_s = -$slope (refs. 22 and 23)]. Apparently, the denser silica formed at psu 20 has a more fractal, rougher surface than the silica formed at psu 33. For *T. weissflogii*, this observation was also made by AFM (Fig. 1 *d* and *h*). For *T. punctigera*, similar observations were made with USAXS (Fig. 2*f*). Scattering of pores of *T. weissflogii* in the SAXS domain ($3 < d < 63$ nm) further revealed an oscillating pattern at low salinity (Fig. 2*d Inset*), indicating that pores were distributed homogeneously. The reorganization of pores may well have been the result of the formation of different smaller pores at psu 20, which we also noticed in the BJH analyses (Fig. 2 *b* and *c*).

Another feature in the (U)SAXS spectra that changed with salinity is the location of the transition points (with radii of gyration (R_g) = $2\pi \cdot Q^{-1}$ in nm) between straight scattering regions, in both cases showing a shift toward higher log$Q$ values and thus lower dimensions (d in nm) at psu 20 (Fig. 2 *d–f* arrowheads). The strongest peak in the biosilica of *T. punctigera* (Fig. 2*f Inset*, marked area) was located at respectively log$Q$ = -1.84 nm $^{-1}$ (psu 33) and log$Q$ = -1.80 nm^{-1} (psu 20) and represented a rather large shift of d from 434 nm to 396 nm. Because the transition points between straight scattering regions are caused by voids (mainly the pores) in the silica (22, 23), the observed upshifts in the Q range of (U)SAXS spectra could be ascribed to a decrease in pore size in silica obtained from cells cultured at psu 20. The calculated radii of gyration for the transition points in the higher log$Q$ region of SAXS spectra corresponded quite well with sizes estimated from the BJH plots (Fig. 2 *b* and *c* and Table 1). The transitions in USAXS spectra and those at lower log$Q$ values in SAXS spectra also agreed with the microscopic observations (Fig. 1 and Table 1). For *T. weissflogii*, the downshift of a pore size of ≈38.5 nm at psu 33 toward 30.0 nm at psu 20 has been calculated from transition points in the upper SAXS spectra (log$Q$ < -0.75; data not shown). This finding also agreed well with estimates made from the BJH plots. In addition, at the lower USAXS domain the shift of pores from a size of ≈72 nm to ≈62 nm was also observed (Fig. 2*e* arrowheads and Table 1). In the lower SAXS region, the pore size shifted from ≈13.5 to ≈10.3 nm (Fig. 2*d* arrowheads). These pores, however, contribute less to the specific pore volume (Fig. 2*b*), possibly because they form the entrance to the sieve-like structure of the much smaller pores (Fig. 1*c*). Results for artificial silicas synthesized at comparable salinities revealed similar nanostructural changes as observed here for the diatom biosilica (Table 1).

The nanostructural analyses showed that the external ionic strength (salinity of the growth medium) affected silica formation in both diatom species. Ionic strength plays an important role in silica sol formation and the subsequent aggregation of sols during polymerization (19, 20). In these processes, lowering of the ionic strength inhibits growth of individual silica sols by enhancing aggregation of smaller ones. The question is whether this chemical rule also is valid in diatom biosilica formation. It has been shown earlier that during growth the biogenic and mineralized silica contents of diatom cells varies, both are affected by salinity (16). In that study, the nanostructure of the biosilica has not been determined, but energy-dispersive x-ray analysis has shown that diatom biosilica at lower salinity contains higher amounts of silicon per probe volume. The presence of a SDV membrane potential (14) and the fact that *in vitro* silica formation mediated by diatomaceous polyamines is strongly induced by (ortho)phosphate are also indicative of a role of ionic strength in diatom silica precipitation. In the *in vitro* silica synthesis studies (9, 10), ionic strength not only determined the aggregation rate but also the size of the silica particles formed: particles became smaller [we suggest: denser, in line with Iler (19)] when the phosphate concentration was lowered. In our chemical syntheses, with artificial seawater in the reaction mixture instead of water, we confirmed that silica becomes denser (Table 1). The role of ionic strength in *in vitro* silica formation seems to be similar to its role *in vivo* formation. It is therefore tempting to propose that the external ion concentration is an important abiotic factor that affects biosilica formation.

In terms of osmoregulation, one should expect that diatom cells compensate for gradients in osmotic pressure to maintain cell turgor and that major cellular processes will not be affected dramatically (15, 24). Indeed, we have shown that growth was not impaired at the two applied culture conditions (Table 1), but the difference of the biosilica nanostructure of cells cultured at higher and lower salinity is evident. Because silicon metabolism in diatoms is independent of the major cellular metabolic pathways for growth [N and P metabolism and photosynthesis (18, 25)], the salinity-dependent nanostructural changes in diatom biosilica could also have occurred without the interference of cellular processes to compensate for differences in osmotic pressure at the applied salinities. In other words, cellular osmoregulatory responses may have had no effect on the silica polymerization reaction inside the SDV. On the assumption that in diatoms silicic acid and other ions of external origin can be taken up simultaneously by the cell [the occurrence of plasmolysis and uptake of necessary reactants in the proximity of the expanding SDV have been suggested earlier (4, 26, 27)], there is no need to invoke intracellular storage and/or transport routes for instance by means of the Golgi apparatus (1). For instance, (macro)pinocytosis (28, 29) favors import of small inorganic reactants from the environment, mitigating the requirement for cellular energy for intracellular stabilization and transport of the chemicals (e.g., silicic acid for diatoms). It has been demonstrated that in diatom biosilica formation the energy requirement is relatively low (30). Simultaneous uptake of extracellular ions and transport into the SDV would also facilitate fast polymerization of silica, a phenomenon demonstrated for *Navicula salinarum* (3). Notice also that silica polymerization reactions do not require much energy once initiated (9, 19, 20, 31).

The hypothesis of import of ions by pinocytosis into the SDV sounds provocative, but it certainly is an option. In diatoms, distinct functions of the outer (distal) and inner (proximal) SDV membranes have been proposed (1) that have resulted from the differences in membrane composition and orientation of the vesicles that fuse with the expanding SDV. Sufficient silicic acid and perhaps silica precursors should have accumulated near the cleavage furrow, triggering cellular pathways (i.e., those related to DNA synthesis (1, 4), to complete cell division and allowing the rapid two-dimensional and subsequent three-dimensional completion of the valve. It has been proposed that the parent frustule itself acts as an antenna for scavenging silicic acid from the environment (4). With respect to nanostructured silica depositioning (so-called micromorphogenesis), the import of external ions into the SDV does not interfere with the proposed branching and phase separation processes in the formation of the pores (4, 6, 7). It is clear that the organic elements playing a role in diatom silica formation have an intracellular origin and must be transported to the SDV and translocated over the silicalemma. It appears that vesicles fuse with the growing SDV. They were previously described as silica transport vesicles [STVs (ref. 32)]. The presence of silica or its precursors inside STVs has, however, never been confirmed, so it seems more likely that STVs deliver membrane parts to the expanding SDV while releasing necessary organic content (e.g., the long-chain polyamines and silaffins) upon fusion. We propose that these vesicles are simply called transport vesicles (TVs; Fig. 3) as long as their content has not been determined accurately.

At present, the exact localization of silicic acid and/or reactive silica precursors at the elevated concentrations that are typical of diatoms cells is under debate. At least five different silicon transporters (SITs) have been identified, and their variation in expression level in the diatom *Thalassiosira pseudonana* has been assessed (6). However, their spatial and temporal localization and that of intracellularly located concentrated silicic acid (and/or silica precursors) have not been elucidated. Because of differences in affinity and/or capacity of SITs to transport silicic acid, diatoms are able to regulate its uptake (6). However, uptake of silicic acid at any location distant from the expanding SDV would require intracellular transport and stabilization of silicic acid and/or silica precursors if only to prevent autopolymerization. Therefore, silicic acid uptake along or in the near vicinity of the distal SDV membrane is more likely (Fig. 3). Diatom cell division is triggered by silicon availability (1), so sufficient silicic acid should become located near the cleavage

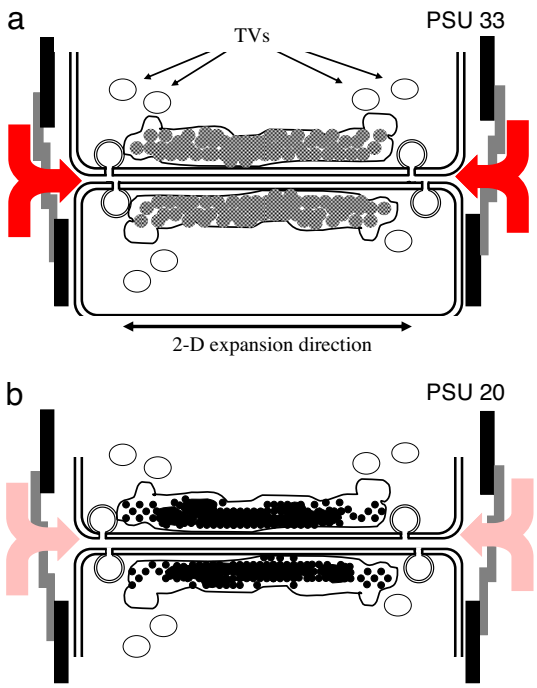

Fig. 3. Schematic presentation of diatom valve formation after cytokinesis of the parental cell at conditions where the external salinity is higher (*a*) and lower (*b*). Based on our data and in line with classical silica chemistry (19, 20), for silica formed under higher salinity, more hydrated silica particles aggregate and coalesce to solid silica (*a*, gray spheres), whereas at lower salinity the same occurs for less hydrated (thus denser) particles (*b*, black spheres). The assumed function of the silicon transport vesicles (1, 31) has been adjusted to simply transport vesicles (TVs) that deliver constituents of cellular origin; most probably membrane parts for the expanding SDV and polypeptides (silaffins, long-chain polyamines) for which it is expected that they accelerate silica precipitation *in vivo* too (9, 10). The occurrence of (macro)pinocytosis (28, 29) and subsequent fusion of these vesicles with the SDV may explain the effect of external ionic strength on the silicification conditions inside the SDV. The influx of ions other than silicic acid increases at higher salinity (*a*, red arrows) and vice versa decreases at lower salinity (*b*, pale red arrows).

furrow if it is true that the diatom cells function as antennas for attracting silicic acid from the environment (4). Eventually, changes in the intercellular space at the cleavage furrow, caused by cellular movements upon cytokinesis and during formation of siliceous cell wall parts, may also facilitate contact with the aqueous extracellular environment for fluid exchange.

Conclusions and Future Directions

The external salt concentration triggers osmoregulation in diatoms, but at the salinity regimes we have applied to *T. punctigera* and *T. weissflogii* this process did not affect growth and did not interfere with silicification. Nevertheless, the observed nanostructural changes indicate that external ionic strength governs diatom biosilica formation in the way described in classical silica chemistry (19, 20); it is apparently independent of physiological processes (18, 25, 30). At the salinity levels usually found offshore (psu >30), diatoms may thus be expected to produce more hydrated, less condensed biosilica (Fig. 3*a*), whereas in more brackish environments near shore diatom biosilica would become less hydrated and packed more dense (Fig. 3*b*). This difference in nanostructure and biogenic silica contents needs to be taken into account by oceanographers and biogeochemists when studying diatom element cycling governed by diatoms in habitats that are affected by salinity changes or salt stratification. To unravel the synergy between both biological and chemical control of diatom biosilica formation, a detailed analysis of the SDV as well as an accurate spatial and temporal localization of its organic and inorganic constituents (and involved transporters) are essential. The alternative route of uptake of silicic acid from the environment by (macro)pinocytosis remains to be assessed. Interestingly, in this respect, the genome sequence of a closely related species, *T. pseudonana* (11), includes genes that encode essential proteins of the pinocytosis machinery.

Materials and Methods

Silica Sources. In obtaining diatom biosilica, the species *T. punctigera* (strain CCRUGTpunct) and *T. weissflogii* (CCRUGTweiss) were cultured in 1-liter polycarbonate flasks (Nalgene, Lima, OH) by using artificial seawater medium (33) with a salinity of 33 and 20 psu, after preadaptation for two generations. The chosen salinities were selected from previous trial experiments (E.G.V. and W.W.C.G., unpublished data) and represent distinct "near-boundary" conditions at which changes in the macromorphology of the frustules were visible without affecting growth rates; in fact, they represent natural values for offshore seawater and brackish areas, respectively. For all cultures, identical amounts of nutrients (882 μM nitrate, 36 μmol of phosphate, and 100 μmol of silicic acid) and culture conditions were applied: a 16-h/8-h light/dark cycle, a light intensity of $\approx$50 μmol photons $\cdot$ $m^{-2} \cdot s^{-1}$ [using Biolux lamps with a spectral range of 390–700 nm (Osram, Munich, Germany)], and a growth temperature of 16°C. Growth was monitored for 7 days followed by harvesting of the cells by centrifugation (5 min at 3,000 $\times$ *g*). Organic matter from the harvested cells was removed by using nitric acid (34) before the silica from the cell walls was further analyzed. Molecular probing studies (3, 14, 35) indicated that the algorithm newSiO$_2$ (%) = 100 (1–0.5^{Tg}) applies to estimate the percentage of silica formed over generations at the applied salinity regimes, in which newSiO$_2$ refers to the newly formed silica at the applied condition between preadaptation and the harvesting day and Tg is the number of generations in that same period. Chemical silica syntheses were performed as described previously (8, 36), but water was replaced by artificial seawater in the reaction mixture to get salinity levels similar to those in the diatom cultures; i.e., psu 33 and psu 20. After the chemical synthesis, the silicas were dried and calcined (2 h at 300°C) before further analysis.

Silica Characterization. AFM images were recorded under a tapping mode (37, 38) on a NTEGRA AFM (NT-MDT, Moscow, Russia), operating in air. A noncontact silicon cantilever, NSG10S (NT-MDT), with a spring force constant of 11–15 N/m was used. Typical resonance frequencies were in the range of 210–230 kHz. HR TEM was performed by using a CM30T electron microscope (Philips; FEI Company, Acht, The Netherlands) equipped with a LaB_6 filament, operating at 300 kV. A few drops of silica samples suspended in ethanol were mounted on a microgrid carbon polymer, which was supported on a copper grid, and allowed to dry in air before examination. The dimensions of mesopores (2–50 nm) in the biosilicas were determined from micrographs, by using an image analysis system (Optimas Co., Edmonds, WA). SAXS, covering a *d* range of 3–63 nm ($0.1 < Q < 2.5$ nm^{-1}, the x-ray wavelength λ = 1.54 Å), was performed on dry acid-cleaned silica at station 8.2 at the Synchrotron Radiation Source, CCLRC (Daresbury, Warrington, U.K.) as described previously (7, 21). USAXS (8, 22, 23), covering a *d* range of 60–6,200 nm ($0.001 < Q < 0.3$ in nm^{-1}, with the x-ray wavelength λ = 0.995 Å), was performed at beamline ID02 at the European Synchrotron Radiation Facility (Grenoble, France). The distribution of pores was measured by the nitrogen adsorption method at liquid nitrogen temperature on a Tri-Star 2000 (Micromeritics Co., Norcross, GA) by using standard continuous procedures. All samples were degassed at 150°C for 3–5 h under reduced pressure before each measure-

ment. The specific surface area and the pore volume contribution were determined, respectively, according to the BET and the BJH methods (21).

We thank Drs. B. U. Komancheck (formerly working at the Synchotron Radiation Source), N. Y. Narayanan (European Synchotron Radiation Facility), and S. A. Alexeev (Department of Chemical Engineering and Chemistry, Eindhoven University of Technology, The Netherlands) for assistance in synchrotron measurements and AFM. This work was supported by Technology Foundation Stichting Technische Wetenschappen Grants Gbc5883 and GFc4983 of the applied science division of Nederlanse Organisatie voor Wetenschappelijk Onderzock and the technology program of the Ministry of Economic Affairs (to E.G.V. and Q.S.), and the Chemical Sciences Division of NWO (to P.J.K.).

1. Pickett-Heaps J, Schmid A-MM, Edgar LA (1990) *Progr Phycol Res* 7:1–168.
2. Round FE, Crawford RM, Mann DG (1990) *Diatoms*: *The Biology and Morphology of the Genera* (Cambridge Univ Press, Cambridge, UK).
3. Hazelaar S, van der Strate HJ, Gieskes WWC, Vrieling EG (2005) *J Phycol* 41:354–358.
4. Gordon R, Drum RW (1994) *Int Rev Cytol* 150:243–372.
5. Hildebrand M, Volcani BE, Gassmann W, Schroeder JI (1997) *Nature* 385:688–689.
6. Hildebrand M (2003) *Progr Org Coat* 47:256–266.
7. Sumper M (2002) *Science* 295:2430–2433.
8. Vrieling EG, Beelen TPM, van Santen RA, Gieskes WWC (2002) *Angew Chem Int Ed* 41:1543–1546.
9. Sumper M, Kröger N (2004) *J Mater Chem* 14:2059–2065.
10. Sumper M, Brunner E (2006) *Adv Funct Mater* 16:17–26.
11. Armbrust EV, Berges JA, Bowler C, Green BR, Martinez D, Putnam NH, Zhou S, Allen AE, Apt KE, Bechner M, *et al*. (2004) *Science* 306:79–86.
12. Robinson DH, Sullivan CW (1987) *Trends Biochem Sci* 12:151–154.
13. Bhattacharyya P, Volcani BE (1980) *Proc Natl Acad Sci USA* 77:6383–6389.
14. Vrieling EG, Beelen TPM, Gieskes WWC (1999) *J Phycol* 35:548–559.
15. Conley DJ, Kilham SS, Theriot E (1989) *Limnol Oceanogr* 34:205–213.
16. Vrieling EG, Poort L, Beelen TPM, Gieskes WWC (1999) *Eur J Phycol* 34:307–316.
17. Tuchman ML, Theriot EL, Stoermer E (1984) *Arch Protistenk* 128:319–326.
18. Claquin P, Martin-Jézéquel V, Kromkamp JC, Veldhuis MJW, Kraaij GW (2002) *J Phycol* 38:922–930.
19. Iler RK (1979) *The Chemistry of Silica* (Wiley, New York), 2nd Ed.
20. Brinker CJ, Scherer GW (1990) *Sol-Gel Science* (Academic, New York).
21. Greg SJ, Sing KSW (1995) *Adsorption*, *Surface Area*, *and Porosity* (Academic, London), 2nd Ed.
22. Vrieling EG, Beelen TPM, van Santen RA, Gieskes WWC (2000) *J Phycol* 35:1044–1053.
23. Vrieling EG, Beelen TPM, Sun Q, Hazelaar S, van Santen RA, Gieskes WWC (2004) *J Mater Chem* 14:1970–1975.
24. Olsen S, Paasche E (1986) *Br Phycol J* 21:183–190.
25. Martin-Jézéquel V, Hildebrand M, Brzezinsky MA (2000) *J Phycol* 36:821–840.
26. Li C-W, Volcani BE (1984) *Phil Trans R Soc London B* 304:519–528.
27. Li C-W, Volcani BE (1985) *Protoplasma* 124:10–29.
28. Seto ES, Bellen HJT, Lloyd E, (2002) *Genes Dev* 16:1314–1336.
29. Liu J, Shapiro JI (2003) *Biol Res Nursing* 5:117–128.
30. Raven JA (1983) *Biol Rev* 58:179–201.
31. Lobel KD, West JK, Hench LL (1996) *Mar Biol* 126:353–360.
32. Schmid A-MM, Schulze D (1979) *Protoplasma* 100:267–288.
33. Veldhuis MJW, Admiraal W (1987) *Mar Biol* 95:47–54.
34. Boyle JA, Pickett-Heaps JD, Czarnecki DB (1984) *J Phycol* 20:563–573.
35. Brzezinski MA, Conley DJ (1994) *J Phycol* 30:45–55.
36. Sun Q, Beelen TPM, van Santen RA, Hazelaar S, Vrieling EG, Gieskes WWC (2002) *J Phys Chem B* 106:11539–11548.
37. Binning G, Quate CF, Gerber C (1986) *Phys Rev Lett* 56:930–933.
38. Radmacher M, Tillmann RW, Fritz M, Gaub HE (1992) *Science* 257:1900–1903.